ENGINEERING Environment
2026, 20(9): 143 https://doi.org/10.1007/s11783-026-2243-4

RESEARCH ARTICLE

Selective addition of ferric hydroxide to Feammox nitrogen transformation favors vivianite formation for phosphorus removal

Xiaohui Cheng[1], Lanlan Hu[1], Xiaotong Cen[2], Tao Liu[3], Xiang Cheng[1], Kangning Xu ✉ [1], Min Zheng ✉ [2]

1. Beijing Key Lab for Source Control Technology of Water Pollution, College of Environmental Science and Engineering, Beijing Forestry University, Beijing 100083, China
2. Water Research Centre, School of Civil and Environmental Engineering, University of New South Wales, Sydney, New South Wales 2052, Australia
3. Department of Civil and Environmental Engineering, The Hong Kong Polytechnic University, Hong Kong 999077, China

HIGHLIGHTS

- Amorphous FeOOH addition in Feammox enables nitrogen and phosphate removal.
- Amorphous FeOOH enhances microbial activity and improves phosphate adsorption.
- Crystalline iron oxide-driving Feammox is less effective for phosphate removal.
- Phosphate removal via vivianite formation is constrained by Fe(II) availability.

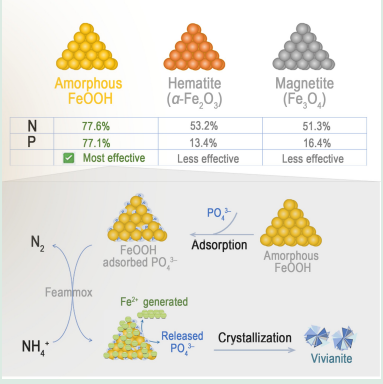

ABSTRACT: Feammox, i.e., anaerobic ammonium oxidation coupled with ferric iron (Fe(III)) reduction, has been considered as a promising option for autotrophic nitrogen removal in wastewater with low carbon/nitrogen ratio. This study proposed a novel technology coupling Feammox and vivianite crystallization for the simultaneous removal of ammonium and phosphate in low-strength wastewater. The results showed that the Feammox process achieved high-level phosphate removal with the selective addition of amorphous ferric oxyhydroxide (amorphous FeOOH) as the iron source, compared to the other iron oxides hematite (α-Fe_2O_3) and magnetite (Fe_3O_4). The removal efficiencies of nitrogen and phosphate reached 77.6% and 77.1%, respectively, with the addition of 0.4 g/L amorphous FeOOH (equivalent to 0.3 g Fe/L). Fundamental investigations through a combination of microscopic images, X-ray diffraction, scanning electron microscopy-energy dispersive spectroscopy, Mössbauer spectroscopy and sequential phosphate extraction method revealed potential mechanisms for phosphate removal. With the addition of amorphous FeOOH, phosphate was firstly adsorbed to mineral surface sites, and then formed vivianite crystals along with microbial Fe(III) reduction (i.e., Feammox reaction) for iron availability. As a result, the Fe(II) formed in Feammox served as a phosphate sink through vivianite precipitation. This study improves the understanding of nitrogen and phosphate transformations in the

✉ Corresponding authors. E-mails: xukangning@bjfu.edu.cn (K. Xu); min.zheng1@unsw.edu.au (M. Zheng)
Article history: Received 28 February 2026, Revised 28 March 2026, Accepted 15 April 2026, Available online 15 May 2026

proposed innovative Feammox-based process and supports the development of next-generation wastewater treatment technologies.

KEYWORDS: Feammox, Vivianite, Autotrophic nitrogen removal, Phosphate removal, Iron

1 Introduction

Iron chemistry is complex and versatile. In the environment, iron occurs predominantly in two redox forms: ferrous iron (Fe(II)) and ferric iron (Fe(III)), occurring in dissolved, colloidal, and particulate forms as redox species such as iron oxides, iron sulfides, iron phosphates, and iron-organic complexes (Kappler et al., 2021). At neutral pH and in the absence of organic ligands, Fe(II) is thermodynamically unstable, while Fe(III) commonly exists as either amorphous (e.g., ferrihydrite) or crystalline phases (e.g., goethite, hematite, and magnetite). The redox-dependent solubility of iron exerts a disproportionate influence on major biogeochemical element cycles and has important environmental applications (Cornell and Schwertmann, 2003; Kappler et al., 2021).

Compared to iron minerals, which are often considered unfavourable iron sources due to their low reactivity, iron salts (e.g., $FeCl_2$, $FeCl_3$, $FeSO_4$, $Fe_2(SO_4)_3$) with better solubility, are widely used in urban water management (Hu et al., 2023a). For instance, iron-based coagulants are employed to remove turbidity and natural organic matter in drinking water treatment plants. In wastewater transport systems, iron salts precipitate sulfide, thereby mitigating odour and corrosion issues in sewers (Cen et al., 2023). Additionally, iron dosing in wastewater treatment plants facilitates phosphate removal and improves sludge settleability and dewaterability (Wilfert et al., 2015). Finally, biogas can be desulfurized by adding iron salts to anaerobic digesters.

Recently, there has been improved knowledge of solid-phase iron minerals application in biological nitrogen removal, particularly through a novel microbial process that couples anaerobic ammonium (NH_4^+) oxidation with Fe(III) reduction, which is an integral part of the iron biogeochemical cycle (Yang et al., 2012; Qin et al., 2024). This process, known as Feammox, contributes to nitrogen loss by anaerobically oxidizing NH_4^+ to nitrogen gas (N_2), nitrite (NO_2^-), or nitrate (NO_3^-) (see Eqs. (1)–(3)) (Yang et al., 2012). Given its advantage of aeration-free and reducing energy consumption by more than 50% compared to conventional nitrogen removal processes, recent studies have focused on enhancing Feammox performance in engineering applications (Nguyen et al., 2023; Zhu et al., 2024). Yang et al. (2018) demonstrated that anaerobic digesters receiving ferric hydroxide ($Fe(OH)_3$), hematite (Fe_2O_3), or magnetite dosing could stimulate Feammox activity, achieving total nitrogen removal efficiencies of 20.1%, 11.3%, and 21.5%, respectively. In a pure culture experiment, Huang and Jaffé (2015) observed higher Feammox activity when using 6-line ferrihydrite ($Fe_5HO_8{\cdot}4H_2O$), a poorly crystalline phase, compared to goethite (α-FeOOH), a well-crystallized mineral.

$$3Fe(OH)_3 + 5H^+ + NH_4^+ \rightarrow 3Fe^{2+} + 9H_2O + 0.5N_2 \quad \Delta_r G_m = -245\ \text{kJ/mol}, \tag{1}$$

$$6Fe(OH)_3 + 10H^+ + NH_4^+ \rightarrow 6Fe^{2+} + 16H_2O + NO_2^- \quad \Delta_r G_m = -164\ \text{kJ/mol}, \tag{2}$$

$$8Fe(OH)_3 + 14H^+ + NH_4^+ \rightarrow 8Fe^{2+} + 21H_2O + NO_3^- \quad \Delta_r G_m = -207\ \text{kJ/mol}. \tag{3}$$

Additionally, the Feammox process drives the transformation of Fe(III), potentially altering mineral identity. In the presence of phosphate in wastewater, the reduction of Fe(III) to Fe(II) is hypothesized to contribute to phosphate removal through the formation of Fe(II) minerals such as vivianite (Wilfert et al., 2015). However, Fe(II) oxidation may also be promoted by Feammox intermediates, such as NO_2^- and NO_3^-, through the nitrate-dependent Fe(II) oxidation (NDFO) process (Cheng et al., 2025). These reduction and oxidation reactions may occur cyclically or simultaneously, which can hinder Fe(II) accumulation and strongly influence the phosphate removal performance. In addition to iron redox reactions, the structural properties of iron oxides, including porosity, specific surface area, and active surface sites, also affect their interactions with phosphate (Wilfert et al., 2015). Amorphous iron oxides with low crystallinity commonly have higher phosphate adsorption capacities than those with high crystallinity, offering a promising approach for phosphate removal (Parfitt et al., 1975; Wang et al., 2013). However, their performance can vary depending on how the iron oxides are produced and applied. Recent studies have shown that the addition of 5 mg Fe/L into an anammox system coupled with partial denitrification enhances both nitrogen and phosphate removal, possibly due to the involvement of Feammox and NDFO in nitrogen conversion and the

coagulant properties of Fe(III) (Kao et al., 2022). Nevertheless, little is known about the phosphate removal performance in Feammox-driven nitrogen transformation systems. Moreover, the effectiveness of different iron oxides in supporting both nitrogen and phosphate removal within such systems has not yet been systematically investigated.

This study aims to investigate the phosphate removal capacity of a Feammox-based nitrogen removal system dosed with solid-phase Fe–O minerals for nitrogen transformation. The effects of long-term, intermittent addition of different Fe–O minerals on nitrogen and phosphate removal performance were evaluated using a laboratory-scale up-flow anaerobic bioreactor operated over 320 d. Feammox activity was initially stimulated by adding 5 mmol/L Fe α-Fe_2O_3, following an operational strategy previously established by our group (Hu et al., 2022), and subsequently dosing with magnetite (Fe_3O_4) and amorphous ferric oxyhydroxide (amorphous FeOOH). Biological ammonium oxidation rate, Fe(II) production rate, and phosphate removal capacity were assessed through batch tests under different Fe–O minerals additions. In addition, iron mineral characterization and microbial community structure were examined throughout the experimental period.

2 Material and methods

2.1 Reactor set-up and operation

An anaerobic bioreactor with a total volume of 1.2 L and an effective reaction zone of approximately 0.76 L was used and described in our previous study (Hu et al., 2022). In brief, wastewater was fed into the bioreactor in an upflow mode via a peristaltic pump (BT100-2J, Longer Pump, China), with treated effluent discharged through gravity overflow. An S-shaped bend was installed on the effluent pipeline to prevent atmospheric air from diffusing into the anaerobic reactor. A three-phase separator was integrated within the bioreactor, which fulfilled dual functions: facilitating sludge sedimentation and return to the reaction zone, and enabling biogas collection into dedicated gas sampling bags. In addition, the influent feeding tank was connected to an auxiliary nitrogen-filled gas bag to maintain an oxygen-free headspace and prevent unintended oxygen intrusion.

Synthetic wastewater was the same as that used in our previous study (Cheng et al., 2025). The influent ammonium (~50 mg N/L) and phosphate (~8 mg P/L) were within the typical range reported for domestic wastewater collected at a local pumping station in St. Lucia, Queensland, Australia (Hu et al., 2023b). A mixture gas of N_2/CO_2 (80%/20%) was flushed in the synthetic wastewater for 30 min to remove dissolved oxygen before feeding into the bioreactor.

Granular anammox sludge, collected from a pilot-scale anammox reactor (Jiangsu, China) dedicated to treating high-strength wastewater, was adopted as the inoculum for this study. After inoculation, hematite (α-Fe_2O_3) was added at a concentration of 5 mmol/L Fe, and the total suspended solids in the laboratory Feammox bioreactor were approximately 3000 mg/L. The air-tight bioreactor was run continuously under ambient temperature (23 ± 3 °C) with a constant hydraulic retention time of 2 d. At the beginning of each phase, different iron minerals were introduced at a concentration of 5 mmol/L Fe, following the sequence: hematite (α-Fe_2O_3) on day 60, magnetite (Fe_3O_4) on day 139, and amorphous ferric oxyhydroxide (FeOOH) on day 200 and 270.

Analytical pure reagents, α-Fe_2O_3 and Fe_3O_4 (Sinopharm Reagent Co., Ltd., China), were used in this study. Amorphous FeOOH was synthesized by dissolving $FeCl_3$ in water and maintaining the pH at 7–7.3 using 1 mol/L NaOH (Lovley and Phillips, 1986). The solid products were collected by centrifugation at 4000 r/min for 10 min (TDL-40B, Anting, China) and washed five times with deionized water.

2.2 Batch assays

To measure and compare the short-term impact of Fe(III) minerals (α-Fe_2O_3, Fe_3O_4, and amorphous FeOOH) on nitrogen and phosphate removal performance, a series of batch tests were carried out in triplicate. Briefly, 90 mL of biomass was collected from the bioreactor and then washed twice with deionized water on day 210. The biomass was equally added into nine 100-mL serum bottles filled with synthetic wastewater deoxygenated by sparging for 30 min with N_2/CO_2 (80%/20%) mixed gas. Each serum bottle was first sealed with a butyl rubber stopper, then pressed tightly with an aluminum cap, and wrapped with tinfoil. The concentrations of ammonium, phosphate, and iron were 50 mg N/L, 65 mg P/L, and 1400 mg Fe/L, respectively. The tests lasted for 36 d, with 5 mL samples collected every 6 days. After each sampling, an equal volume of N_2/CO_2 (80%/20%) gas was injected to maintain pressure balance. Another series of abiotic batch tests was included to investigate phosphate removal through adsorption by amorphous FeOOH, with the initial concentrations of phosphate and amorphous FeOOH of 65 mg P/L and 1400 mg Fe/L,

respectively. The ammonium removal rate and Fe(II) production rate were calculated using linear regression of ammonium and Fe(II) concentrations during the batch tests.

2.3 Water quality analysis

Solution pH and dissolved oxygen (DO) were measured using a laboratory benchtop pH meter (Leici E-301F, Shanghai INESA & Scientific Instrument, China) and a portable DO analyzer (Oxi3310, WTW, Germany), respectively. Concentrations of ammonium, nitrite, nitrate and phosphate were quantified via colorimetric methods with an ultraviolet-visible spectrophotometer (DR 3900, HACH, USA), in accordance with the standard protocols specified in Standard Methods for the Examination of Water and Wastewater (APHA, 1998).

2.4 Iron analysis

Aqueous Fe(II) concentration was quantified via the 1,10-phenanthroline colorimetric method using a DR3900 spectrophotometer with USEPA-certified Hach reagents. Total Fe concentration was determined using Hach test kits containing hydroxylamine hydrochloride, which reduces all Fe(III) in the samples to Fe(II) for subsequent colorimetric analysis. Fe(III) concentration was then derived by subtracting the measured Fe(II) concentration from the total Fe value. To mitigate the oxidative loss of Fe(II) prior to analysis, all water samples collected for Fe(II) measurement were immediately acidified to pH 2 upon sampling. Sludge samples were pretreated before the measurement of Fe(II) and total Fe. In brief, 0.8 mL sludge sample was subjected to extraction with 4.0 mL of 3.6 mol/L hydrochloric acid for 16 h at ambient temperature, a treatment designed to solubilize total Fe in the sample. Following the iron extraction procedure, the resulting solution was filtered through a 0.45 μm polyethersulfone membrane (TGMF60, Jinteng, China) to remove solid particulates, with the filtrate collected for subsequent instrumental analysis.

2.5 Characterization of solid samples

The morphology of sludge samples on days 0, 210, and 310 was examined using a digital microscope (Smart 320, Optec, China). Moreover, the samples collected on days 210 and 310 were dried and sealed in oxygen-free 50-mL brown centrifuge tubes, with oxygen removed by flushing N_2 for 2 min before further analysis. The samples were characterized via a scanning electron microscopy coupled with energy dispersive spectroscopy (SEM-EDS) with a field-emission scanning electron microscope (SU8010, Hitachi, Japan) integrated with an EDS detector, which allowed for the systematic observation of microstructural features, surface morphologies and elemental composition of the samples. X-ray diffraction (XRD) measurements were carried out on a Shimadzu XRD-7000 diffractometer, employing Cu Kα radiation operated at 40 kV and 40 mA, and the scanning was performed at a rate of 5° per minute over the 2θ range of 5°−80°. Fe mineral species and their relative contents were identified via Mössbauer spectroscopy, with ^{57}Fe Mössbauer absorption spectra acquired at 300 K using a Topologic 500A spectrometer equipped with a Rh (^{57}Co) radiation source. The obtained Mössbauer spectra were subsequently processed and fitted using the Mosswinn 3.0i data analysis software package. Additionally, phosphate fractions in the bottom and fully mixed sludge collected on day 310 were analyzed using sequential phosphate extraction, as described in Text S1.

2.6 High-throughput sequencing of 16S rRNA gene amplicons

Genomic DNA was extracted from 10 mL biomass sludge samples collected on days 0, 90, 164 and 267 using the E.Z.N.A. Soil DNA Kit (Omega Bio-Tek Inc., USA), strictly following the manufacturer's operational protocols. The purity and concentration of the extracted DNA were quantified with a Nanodrop UV-visible spectrophotometer (Thermo Fisher Scientific, USA). The V3-V4 hypervariable regions of the 16S rRNA gene were amplified from the purified DNA via polymerase chain reaction (PCR) on a Gene Amp 9700 system (ABI, USA), using the universal primer pair 338F (5-ACTCCTACGGGAGGCAGCAG-3) and 806R (5-GGACTACHVGGGTWTCTAAT-3). PCR amplicons were separated by 2% agarose gel electrophoresis, and the target bands were excised and purified with the AxyPrep DNA Gel Extraction Kit (Axygen Biosciences, USA) in accordance with the kit's instructions; the purified products were then quantified using a Quantus^{TM} Fluorometer (Promega, USA). All qualified purified amplicons were subjected to high-throughput sequencing on an Illumina MiSeq PE300 platform (Illumina, USA), with the sequencing experiments and raw data processing conducted by Majorbio Bio-Pharm Technology Co. Ltd. (Shanghai, China) following standard laboratory protocols.

2.7 Statistical analysis

All experimental data were subjected to statistical

analysis using the SPSS 27.0 software package by one-way ANOVA with least significance difference test. Significant difference among different treatments was analyzed with a significant threshold p-value of 0.05.

3 Results and discussion

3.1 Long-term reactor performance

The Feammox bioreactor was continuously operated for ~320 d, with five separate additions of different ferric compounds (Fig. 1(a)). Initially, the effluent ammonium concentration gradually decreased after the first dosing of α-Fe_2O_3, establishing an ammonium removal efficiency of 59.6% on day 17 but declined thereafter (Fig. 1(a)). After re-dosing α-Fe_2O_3 on day 60, the ammonium removal efficiency rebounded and stabilized at 53.2% ± 6.8% during 89–138 d, which is comparable to the 53% removal efficiency reported in a previous study under similar operating conditions (Hu et al., 2022). During the subsequent addition of Fe_3O_4 (139–199 d), the ammonium removal efficiency remained stable, averaging 51.3% ± 7.8%. Intriguingly, with the addition of amorphous FeOOH on day 200 and day 270, the ammonium removal capacity significantly ($p < 0.05$) increased. The efficiency reached 77.6% ± 5.0 %, about one-third higher than that achieved with α-Fe_2O_3 and Fe_3O_4. These results suggest that amorphous FeOOH addition is favorable for promoting Feammox reactions. Throughout the long-term operation, the concentration of nitrite in the effluent remained low (~0.2 mg N/L) and nitrate levels were approximately 7.8 ± 3.6 mg N/L (Fig. 1(a)).

Figure 1(b) shows the phosphate profiles in the Feammox bioreactor under different iron mineral additions. With an influent concentration of 7.8 ± 0.4 mg P/L, the effluent phosphate concentration gradually decreased following the addition of various iron compounds. When α-Fe_2O_3 was used as the ferric source, the phosphate removal efficiency was low, at 13.4% ± 4.1%, and only slightly improved to 16.4% ± 2.2% with Fe_3O_4 addition (Fig. 1(c)). In contrast, the effluent phosphate concentration substantially decreased following the addition of amorphous FeOOH, achieving a removal efficiency of 77.1% ± 8.2% during day 289–314. The effluent total ferrous concentration was 11.1 ± 8.1 mg Fe/L (Fig. 1(d)), indicating the loss of iron with the effluent. The XRD patterns of these three added iron minerals (Fig. S1) revealed that synthesized amorphous FeOOH, an intermediate between 2-line and 6-line ferrihydrite (Wang et al., 2024), has lower crystallinity than the purchased α-Fe_2O_3 and Fe_3O_4. In general, iron compounds with lower crystallinity exhibit larger specific surface areas and faster dissolution kinetics

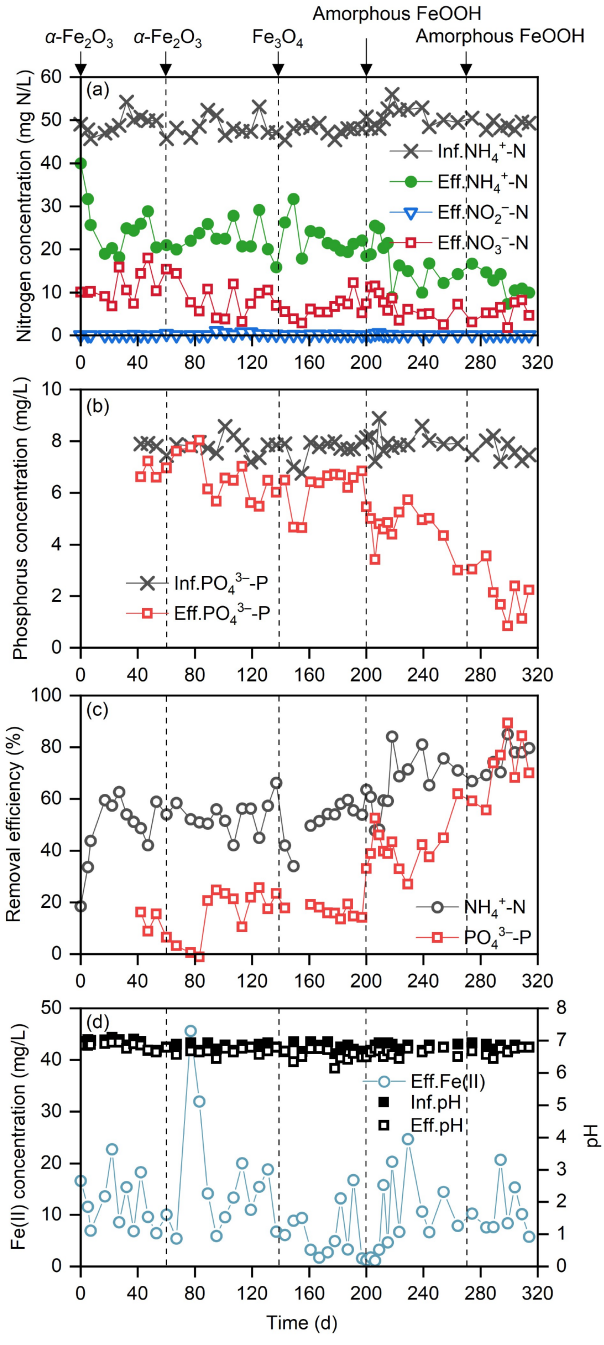

Fig. 1 Nitrogen and phosphate profiles of the bioreactor: (a) influent ammonium concentration and effluent ammonium, nitrite, and nitrate concentration; (b) phosphate concentration in influent and effluent; (c) ammonium and phosphate removal efficiency; (d) influent and effluent pH, and effluent Fe(II) concentration. Arrows indicate the addition of iron sources to the Feammox bioreactor.

relative to highly crystalline ferric phases (Wilfert et al., 2015; Yang et al., 2018), which may enhance their bioavailability for microorganisms and their capacity for phosphate removal (Wang et al., 2023). As a consequence, using amorphous FeOOH as an iron source appeared to promote both Feammox activity and phosphate removal in the bioreactor.

3.2 Effect of iron minerals on nitrogen and phosphate removal

Three groups of batch tests were conducted using the Feammox biomass collected from the bioreactor on day 210, to compare the impact of α-Fe_2O_3, Fe_3O_4, and amorphous FeOOH additions on nitrogen and phosphate removal. The results were presented in Figs. 2(a), 2(b) and 2(c), respectively. In all the tests, the decrease in ammonium was accompanied by Fe(II) generation, indicating the presence of Feammox activity. The ammonium removal rate in the α-Fe_2O_3 group (0.50 ± 0.03 mg N/(L·d)) was similar to that in the Fe_3O_4 group (0.50 ± 0.01 mg N/(L·d)) (Fig. 2(d)). It was improved by 24% in the amorphous FeOOH group (0.62 ± 0.04 mg N/(L·d)). This is consistent with the long-term bioreactor operations, confirming that amorphous FeOOH is more favorable for N removal than α-Fe_2O_3 and Fe_3O_4.

The rates of Fe(II) formation were 0.85 and 1.28 mg/(L·d) in α-Fe_2O_3 and Fe_3O_4 group, respectively. Fe_3O_4 ($Fe^{II}Fe_2^{III}O_4$) stoichiometry theoretically yields an Fe(II)/Fe(III) ratio of 0.5, which could explain its higher Fe(II) formation rate despite exhibiting a similar ammonium removal rate to that of the α-Fe_2O_3 group. The Fe(II) formation rate in the biotic assays with amorphous FeOOH was 1.67 mg/(L·d), further confirming that the amorphous FeOOH promotes Feammox activity. The Fe(II) generation rate in this system is substantially lower than that (2.8–6.4 mg/(L·d)) observed in heterotrophic systems (González et al., 2025). This discrepancy is likely associated with the enhancement of microbial Fe(III) reduction by organic substrates, suggesting that organic matter availability may represent a key factor limiting Fe(II) production.

The concentration of phosphate gradually decreased from 66.6 to 55.0 mg P/L with the addition of α-Fe_2O_3 and from 68.9 to 54.1 mg P/L with Fe_3O_4 over 35 d, with both showing slow removal rates (Figs. 2(a) and 2(b)). In these batch tests, the phosphate adsorption on α-Fe_2O_3 and Fe_3O_4 could be neglected because highly crystallized iron oxides commonly have relatively low

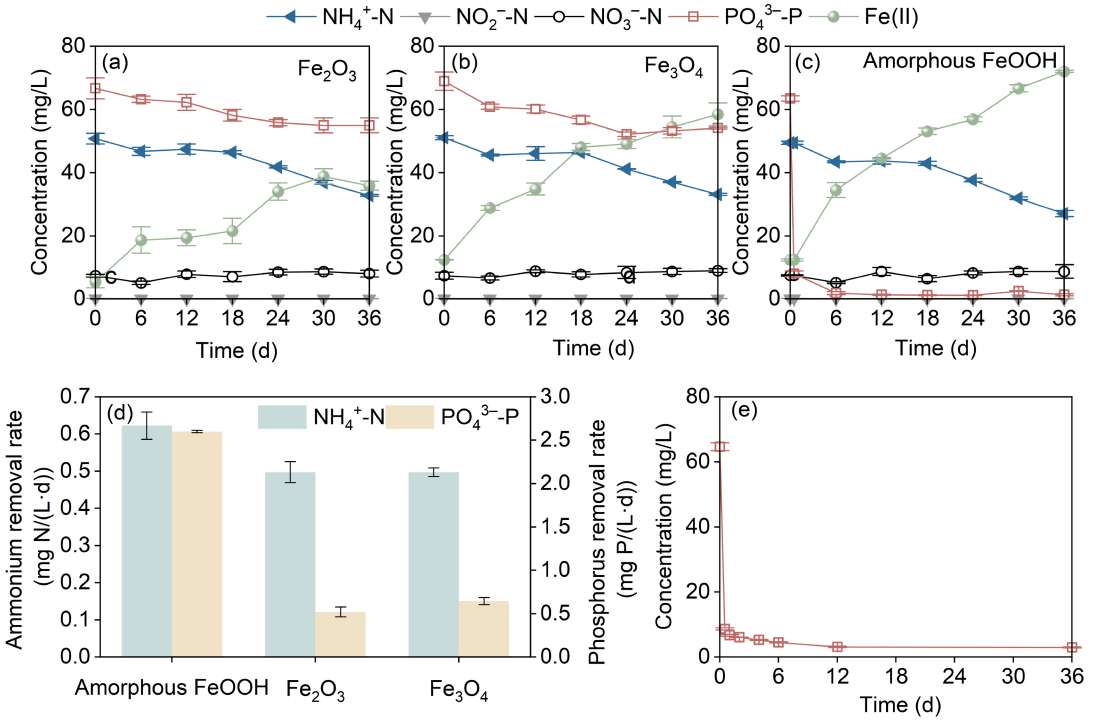

Fig. 2 Concentrations of ammonium, nitrite, nitrate, phosphate, and total Fe(II) in biotic batch tests by adding α-Fe_2O_3 (a), Fe_3O_4 (b), and amorphous FeOOH (c). Estimated ammonium and phosphate removal rates in different treatments (d). Phosphate concentration in the abiotic control test with the addition of amorphous FeOOH (e).

phosphate adsorption ability (Lin et al., 2023). Microbial reduction of Fe(III) in Feammox could result in the formation of Fe(II) from these iron minerals and might subsequently facilitate phosphate removal through the formation of insoluble minerals such as vivianite (Rasmussen and Nielsen, 1996).

However, in the group of amorphous FeOOH addition, phosphate concentration substantially decreased from 63.4 to 7.95 mg P/L within 12 h, and further to 1.76 mg P/L within 6 d (Fig. 2(c)). These results indicate a significantly greater phosphate removal capacity by Feammox sludge when amorphous FeOOH was selectively added, consistent with observations from long-term bioreactor operation. Abiotic control tests, in which amorphous FeOOH was added to the phosphate solution, validated its high phosphate removal capacity (Fig. 2(e)). A rapid decrease in phosphate concentration was observed within 12 h, corresponding to a removal rate of approximately 112 mg P/(L·d), similar to the rate observed in biotic tests (~111 mg P/(L·d)). However, the adsorption rate was significantly lower than the values (0.176–0.713 mg P/(mL·min)) reported in the previous study (Xu et al., 2022), which may be attributed to the rapid attainment of adsorption equilibrium within 12 h. These results indicated that physicochemical process was the primary mechanism governing phosphate removal. As known, amorphous FeOOH is a strong phosphate adsorbent due to its low crystallinity and surface hydroxyl groups that can provide reactive sites for adsorption (Cornell and Schwertmann, 2003). The phosphate adsorption capacity of amorphous FeOOH observed in this study was 25 mg/g Fe oxide, consistent with the literature (20 mg P/g Fe oxide at pH 10; 29 mg P/g Fe oxide at pH 3.5) (Parfitt et al., 1975). Notably, the phosphate concentration in the abiotic control tests reached 4.43 mg P/L, while it decreased to 1.76 mg P/L in biotic tests by day 6. This difference may be attributed to microbial reduction of Fe(III) under anaerobic conditions and the resulting Fe(II) may subsequently improve the phosphate removal through vivianite formation (Rasmussen and Nielsen, 1996). Consistent with mechanisms observed in natural systems, previous studies have suggested that Fe oxides with pre-adsorbed phosphate can serve as precursor phases for vivianite formation, as observed in lake and intertidal sediments amended with phosphate-loaded Fe oxides (Heinrich et al., 2021; Kubeneck et al., 2025).

3.3 Iron speciation in sludge

XRD analysis of sludge samples collected on days 210 and 310 identified four iron species: the three dosed iron minerals (α-Fe_2O_3, Fe_3O_4 and amorphous FeOOH), and phosphate mineral vivianite (Fig. 3). In addition, EDS analysis estimated an Fe:P atomic ratio of 1.99 (Fig. S2), which is slightly higher than the theoretical stoichiometric Fe:P ratio of 1.5:1 in vivianite (Deng et al., 2020). This indicates the presence of other iron compounds in the Feammox sludge, e.g., the dosed iron minerals, and indicates that vivianite precipitation may not be the sole mechanism responsible for phosphate removal. This finding is consistent with the results observed in the batch tests (Section 3.2) and the phosphate distribution analysis of the bottom sludge (Fig. S3), where 44.82% of phosphate was identified as vivianite, while the remaining 55.18% was associated with ferric phosphate and other Fe(III) compounds, such as amorphous FeOOH, primarily through adsorption.

The XRD patterns also revealed a transition from an amorphous composition to a more crystalline form of vivianite, as evidenced by the appearance of sharp vivianite peaks in the day 310 sample. This finding was

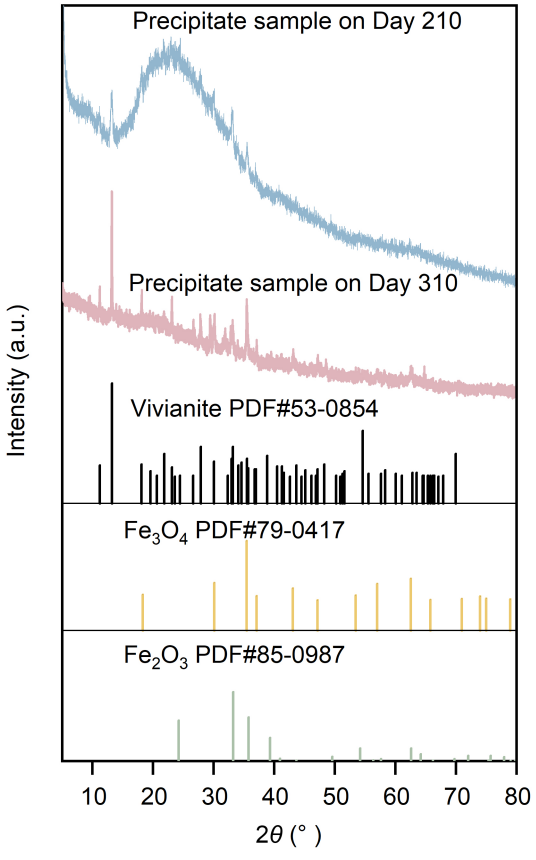

Fig. 3 XRD patterns of the sludge in the bioreactor sampled on days 210 and 310 in comparison to standard XRD patterns of vivianite, Fe_3O_4 and α-Fe_2O_3.

supported by the microscopic images (Figs. 4(a)–4(c)) and SEM analyses, which showed the change in mineral morphology, from undetectable solid phases on day 0 to increasingly amorphous and crystalline structures on days 210 and 310. The solid mineral closely matched the standard reference materials for amorphous FeOOH colloid and vivianite crystals (Fig. 4(d)), with particle sizes ranging from 10 to 50 μm (Figs. 4(e) and 4(f)). Combined, these results suggested that the accumulated iron and phosphate promoted vivianite formation in the Feammox bioreactor.

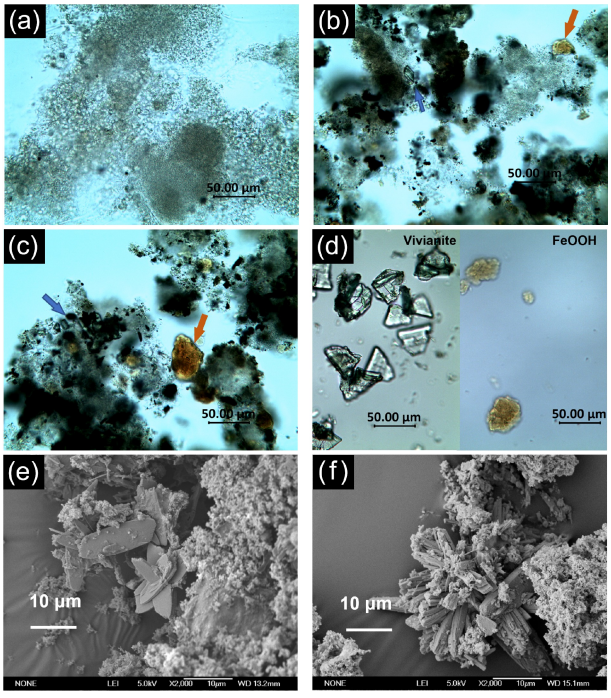

Fig. 4 Microscopic images of Feammox sludge particulates on day 0 (a), day 210 (b), day 310 (c), and chemically synthesized vivianite and amorphous FeOOH (d). Dark blue arrows: vivianite; light yellow arrows: amorphous FeOOH. SEM image of solid products collected on days 210 (e) and 310 (f).

Mössbauer spectroscopy was performed on the sludge sampled on day 310 to identify iron compounds present in the sludge (Table 1 and Fig. S4). The results revealed that 22% and 24% of the total iron existed as Fe(II)-vivianite and Fe(III)-vivianite, respectively. Considering the potential oxidation of Fe(II) during sample preparation, or auto-oxidation (Pratt, 1997), as well as the pseudo anaerobic conditions (~0.05 mg/L, Fig. S5) and nitrate (~8 mg N/L) present in the bioreactor (Carlson et al., 2013; Deng et al., 2020), the total vivianite content was estimated to be approximately 46% of the solid-phase iron. The remaining iron species included magnetite (12%), hematite (8%), and other Fe(III) compounds (34%). Mössbauer spectroscopy analysis at 300 K were sufficient to quantify the dominant Fe-bearing phases (especially vivianite-related fractions). However, 77 and 4 K measurements can resolve finer details of poorly crystalline and crystalline Fe-oxide phases, e.g., ferrihydrite and lepidocrocite. The low-temperature Mössbauer spectroscopy analysis could be a priority for refined minor Fe-phase quantification for the research on iron redox in Feammox in future work.

3.4 Dynamics of the microbial communities

Analysis of the microbial community structure (Fig. S6) demonstrated a pronounced reduction in the relative abundance of the anammox bacterium *Candidatus Brocadia*, falling from 23.3% in the inoculum sludge to only 1.29% by day 267. This suggests that anammox bacteria may not play an important role in N removal of the bioreactor, despite their known to use insoluble Fe as extracellular electron acceptors (Yang et al., 2021). In contrast, the total relative abundances of dissimilatory iron reduction bacteria (DIRB), as potential Feammox strains (Table S1), e.g., *Clostridium*, *Thiobacillus*, *Ignavibacterium*, and

Table 1 Mössbauer parameters derived from the spectra collected at 300 K for the sludge sampled on day 310 from the Feammox bioreactor

Subspectrum	Isomer shift (mm/s)	Quadrupole splitting (mm/s)	Line width (mm/s)	Hyperfine field	Phase	Contribution (%)
1	0.460	0.767	0.270	–	Fe(III) (Viv. A+B)	24
2	1.170	2.470	0.469	–	Fe(II) (Viv. A)	11
3	1.183	2.976	0.270	–	Fe(II) (Viv. B)	11
4	0.246	0.043	0.283	48.98	Magnetite A	4
5	0.687	−0.072	0.509	45.59	Magnetite B	8
6	0.325	−0.188	0.328	51.34	Hematite	8
7	0.269	0.755	0.306	–	Fe(III) (other)	34

Note: Vivianite A and B represent Fe(II) ions located at the Fe1 and Fe2 crystallographic sites within the vivianite crystal structure, respectively. Magnetite A and B denote Fe(III) on the A site and Fe(II) and Fe(III) on the B site. Reduced chi-square χ^2 (1.341) ≈ 1, meaning that the fit is good and the model is reasonable.

Paludibaculum (Dedysh et al., 2021; Xu et al., 2024), significantly increased from 0.74% in the seed sludge to 9% on day 267, indicating their potential contribution to N removal (Table 2). Notably, the relative abundances of DIRB on day 267 following the addition of amorphous FeOOH (9%) was higher than that observed on day 90 with α-Fe_2O_3 (3.62%) and day 164 with Fe_3O_4 (2.94%). This trend aligns with the N removal efficiencies observed for the addition of various Fe(III) sources.

3.5 Outlook

While recent studies have explored Feammox performance with different iron types (Huang and Jaffé, 2015; Yang et al., 2018), their roles in phosphate removal performance within Feammox system remain largely uninvestigated. This study demonstrates that amorphous FeOOH can selectively achieve simultaneous removal of up to 77% of both nitrogen and phosphate. In contrast, Fe_3O_4 and α-Fe_2O_3 supported nitrogen removal via the Feammox process at 51.3% and 53.2%, but exhibited limited phosphate removal efficiency of only 16.4% and 15.9%, respectively. On the one hand, amorphous FeOOH rapidly adsorbs phosphate through electrostatic attraction, as its positively charged surface interacts with negatively charged phosphate ions. On the other hand, Feammox-based nitrogen transformation produces ferrous ions, which can precipitate with phosphate to form vivianite, a stable, solid-phase phosphate product in sludge. Integrated analysis using microscopic images, XRD, SEM-EDS and Mössbauer spectra conform that the phosphate removal in the presence of amorphous FeOOH occurs through a combination of surface adsorption and vivianite crystallization. However, for the highly crystalline Fe_3O_4 and α-Fe_2O_3, phosphate removal primarily occurred through the release of iron generated by Fe(III) reduction and subsequent formation of vivianite. This was supported by the molar ratio of produced Fe(II) to removed phosphate (ΔFe(II)/ΔP), which was 1.45 for α-Fe_2O_3 and 1.73 Fe_3O_4, both close to the stochiometric Fe(II)/P ratio of vivianite (1.50).

Overall, the maximum ammonium removal efficiency achieved in this study was 77.6% ± 5.0%, which is comparable to that (~80%) reported in a similar study employing continuous dosing of soluble $FeCl_3$ with the influent (Li et al., 2018). However, this value was lower than the ammonium removal efficiency (~97%) reported in a study using $Fe(OH)_3$ as the iron source (Cheng et al., 2025). Notably, that study focused exclusively on nitrogen removal, whereas the present study was designed to achieve simultaneous nitrogen and phosphorus removal. Similarly, although phosphate removal efficiencies of up to ~98% have been reported in a previous study involving organic supplementation

Table 2 Relative abundances of potential Feammox genera in the sludge samples collected from the bioreactor on days 0, 90, 164 and 267

Genus	Day 0 (%)	Day 90 (%)	Day 164 (%)	Day 267 (%)
Pseudomonas	0.22	1.18	0.11	0.14
Geothrix	0	0	0.01	0.06
Geobacteraceae_unclassified	0	0.23	0.13	0
Paludibaculum	0	0.83	2.15	1.69
Ignavibacterium	0.22	0.19	0.13	1.53
Clostridium	0.08	0	0.07	4.86
Desulfovibrio	0	0.3	0.01	0.02
Bacillus	0.01	0	0	0.03
Thiobacillus	0.07	0.1	0.05	0.12
Sphingomonas	0	0.05	0	0.01
Rhodobacter	0.01	0.01	0	0
Acinetobacter	0	0.05	0	0.02
Thermomonas	0.1	0.1	0.07	0.08
Paenibacillus	0	0	0	0
Achromobacter	0	0.03	0	0.01
Rhodanobacter	0.03	0.55	0.21	0.43
Total	0.74	3.62	2.94	9

(Dou et al., 2022), direct comparison is challenging due to differences in reactor configuration and carbon availability. In the present study, the phosphate removal efficiency was comparable to that reported (~78.7%) for PN/A systems with iron addition under organic-free conditions (Kao et al., 2022). The presence of organic substrates can enhance microbial Fe(III) reduction and promote Fe(II) accumulation, thereby facilitating phosphate immobilization. Under the low C/N conditions applied in this study, phosphate removal was likewise iron-mediated but relied predominantly on iron mineral transformation and surface reactivity rather than on organic-enhanced iron reduction. This indicates that effective phosphate immobilization can be achieved through intrinsic iron cycling even in the absence of organic supplementation, highlighting the robustness of the iron-mediated strategy for simultaneous nitrogen and phosphorus removal.

The theoretical value of Fe∶N in Feammox reactions ranges from 3 to 8 determined by the product of ammonium oxidation according to Eqs. (1)–(3), meaning that the lowest Fe∶N ratio required to remove N via Feammox is 3∶1. In contrast, the actual molar ratio of consumed Fe (i.e., produced Fe(II)) to removed N was only 0.12∶1, accounting for only 4% of the demand of Fe(III) in Feammox. The reason may be due to the formation of Fe(III) via the NDFO processes (Eqs. (4)–(5)) (Hu et al., 2022) and the chemical Fe(II) oxidation by oxygen in the bioreactor (Pan et al., 2025). If the oxidation and reduction reactions occur cyclically or simultaneously, the availability of Fe(II) for phosphate removal through vivianite precipitation may be reduced. This further explains why, during the crystalline Fe_3O_4 and α-Fe_2O_3 addition phase, phosphate removal efficiency is 0.8 times lower than that that achieved with amorphous FeOOH which may remove phosphate through adsorption and co-precipitation mechanisms.

$$10Fe^{2+} + 12H^{+} + 2NO_3^{-} \rightarrow 10Fe^{3+} + 6H_2O + N_2$$
$$\Delta_r G_m = -457\ \text{kJ/mol}, \quad (4)$$

$$6Fe^{2+} + 8H^{+} + 2NO_2^{-} \rightarrow 6Fe^{3+} + 4H_2O + N_2$$
$$\Delta_r G_m = -438\ \text{kJ/mol}. \quad (5)$$

It should be noted that the results were obtained using laboratory reactors treating synthetic wastewater without organic matter. In real wastewater, the presence of organic matter is likely to support heterotrophic dissimilatory iron-reducing bacteria, often referred to as iron-mineral-dissolving microorganisms, which can promote the dissolution of iron minerals and enhance phosphate removal through vivianite precipitation (Liu et al., 2025). Additionally, repeated iron redox cycling may gradually reduce the crystallinity of iron minerals, thereby increasing their phosphate adsorption capacity (Wilfert et al., 2015; Kappler et al., 2021). Meanwhile, a few studies have investigated the impact of organic matter on nitrogen removal via the Feammox process. For instance, Nguyen et al. (2023) reported that ammonia removal efficiency decreased from 99% to 50% in a Feammox bioreactor when the influent C/N ratio increased from 2.5 to 5.6. In contrast, Le et al. (2021) found that a C/N ratio of 1.4 yielded the highest ammonia removal efficiency (98.3%), compared to 85.5% and 83.3% at C/N ratios of 0.7 and 1.1, respectively. These conflicting findings may be attributed to the dual role of organic matter (Liu et al., 2025): (1) promoting dissimilatory iron reduction, which competes with Feammox for Fe(III), and (2) supporting heterotrophic denitrification, which may enhance overall nitrogen removal by reducing residual nitrate. It is hypothesized that by managing the balance of organic matter and ensuring a sufficient supply of iron, simultaneous nitrogen and phosphate removal may be achievable in Feammox systems treating domestic wastewater with low organic content (Liu et al., 2025).

A key limitation of the present study is the intentional exclusion of sulfate from the synthetic wastewater, despite this enables revealing the mechanisms of Feammox-mediated nitrogen and phosphorus removal without confounding interferences. However, this inevitably reduces the direct real-world relevance of the findings to actual municipal wastewater. Sulfate might exert bidirectional and complex effects on the Feammox system. Firstly, sulfate can drive sulfate-dependent anaerobic ammonium oxidation (Sulfammox) to compete with Feammox for ammonium as electron donor. Although thermodynamic analysis suggests that Feammox is more prone to occur than Sulfammox, previous studies have shown that both can be carried out simultaneously in the same reactor (Ye et al., 2025). The reduction product sulfide could directly compete with phosphate for Fe(II) via FeS precipitation, which could theoretically inhibit vivianite formation and reduce the removal of phosphate. Secondly, oxidants including nitrate and Fe(III) present in the reactor might re-oxidize sulfide back to sulfate (Chen et al., 2025) and release Fe(II) from the FeS precipitates, thereby partially restoring Fe(II) availability for phosphate removal. Given the complex coupling of sulfur, nitrogen, iron, and phosphorus cycles triggered by sulfate, the impact of sulfate on this Feammox-based process should be addressed using real wastewater in further studies.

4 Conclusions

This study demonstrated enhanced phosphate removal during the Feammox nitrogen conversion process when selectively using amorphous FeOOH as an iron source, compared to Fe_3O_4 and α-Fe_2O_3. Two primary mechanisms contributed to phosphate removal by the tested iron oxides: surface adsorption and vivianite precipitation. The former is influenced by the mineral phase and structure, with amorphous FeOOH, a short-range-ordered mineral, exhibiting a greater phosphate adsorption capacity than the more crystalline Fe_3O_4 and α-Fe_2O_3. The latter mechanism depends on the availability of Fe(II), which may be limited by competing redox reactions. In addition to improved phosphate removal, amorphous FeOOH also supported faster ammonium oxidation and higher total nitrogen removal efficiency than the more crystalline iron oxides, indicating that mineral structure plays a critical role in microbial Feammox activity. These findings highlight the importance of selecting appropriate iron sources to optimize nutrient removal. For future applications in domestic wastewater treatment, amorphous FeOOH offer a promising, cost-effective solution for achieving integrated nitrogen and phosphate removal and recovery.

Conflicts of Interest The authors declare that they have no known competing financial interests or personal relationships that could have appeared to influence the work reported in this paper.

Acknowledgements This study was supported by the National Natural Science Foundation of China (No. 52270022) at Beijing Forestry University. M.Z. acknowledges the support of Australian Research Council (ARC) Industry Fellowship (No. IE230100245) and ARC Linkage Grant (No. LP230101054).

Electronic Supplementary Material Supplementary material is available in the online version of this article at https://dx.doi.org/10.1007/s11783-026-2243-4 and is accessible for authorized users.

Funding Note Open Access funding enabled and organized by CAUL and its Member Institutions.

References

Carlson H K, Clark I C, Blazewicz S J, Iavarone A T, Coates J D (2013). Fe(II) oxidation is an innate capability of nitrate-reducing bacteria that involves abiotic and biotic reactions. Journal of Bacteriology, 195(14): 3260–3268

Cen X T, Li J L, Jiang G M, Zheng M (2023). A critical review of chemical uses in urban sewer systems. Water Research, 240: 120108

Chen S C, Li X M, Battisti N, Guan G Q, Montoya M A, Osvatic J, Pjevac P, Pollak S, Richter A, Schintlmeister A, et al. (2025). Microbial iron oxide respiration coupled to sulfide oxidation. Nature, 646(8086): 925–933

Cheng X H, Hu L L, Liu T, Cheng X, Li J Y, Xu K N, Zheng M (2025). High-level nitrogen removal achieved by Feammox-based autotrophic nitrogen conversion. Water Research X, 27: 100292

Cornell R M, Schwertmann U (2003). The Iron Oxides: Structure, Properties, Reactions, Occurrences and Uses. Weinheim, Germany: Wiley-VCH, xxxix + 664 pp

Dedysh S N, Beletsky A V, Kulichevskaya I S, Mardanov A V, Ravin N V (2021). Complete genome sequence of *Paludibaculum fermentans* P105^T, a facultatively anaerobic acidobacterium capable of dissimilatory Fe(III) reduction. Microbiology Resource Announcements, 10(1): e01313–20

Deng S Y, Zhang C Y, Dang Y, Collins R N, Kinsela A S, Tian J B, Holmes D E, Li H S, Qiu B, Cheng X, et al. (2020). Iron transformation and its role in phosphorus immobilization in a UCT-MBR with vivianite formation enhancement. Environmental Science & Technology, 54(19): 12539–12549

Dou Q H, Zhang L, Lan S, Hao S W, Guo W, Sun Q X, Wang Y P, Peng Y Z, Wang X Y, Yang J C (2022). Metagenomics illuminated the mechanism of enhanced nitrogen removal and vivianite recovery induced by zero-valent iron in partial-denitrification/anammox process. Bioresource Technology, 356: 127317

González H, Rodríguez C, González M, González C, Serrano J, Leiva E (2025). Ammonium and organic carbon co-removal under Feammox heterotrophic conditions at low Fe^{3+} concentrations. Bioresource Technology, 434: 132750

Heinrich L, Rothe M, Braun B, Hupfer M (2021). Transformation of redox-sensitive to redox-stable iron-bound phosphorus in anoxic lake sediments under laboratory conditions. Water Research, 189: 116609

Hu L L, Cheng X H, Qi G X, Zheng M, Dang Y, Li J Y, Xu K N (2022). Achieving ammonium removal through anammox-derived Feammox with low demand of Fe(III). Frontiers in Microbiology, 13: 918634

Hu Z T, Li L Q, Cen X T, Zheng M, Hu S H, Wang X H, Song Y R, Xu K N, Yuan Z G (2023a). Integrated urban water management by coupling iron salt production and application with biogas upgrading. Nature Communications, 14(1): 6405

Hu Z T, Liu T, Wang Z Y, Meng J, Zheng M (2023b). Toward energy neutrality: novel wastewater treatment incorporating acidophilic ammonia oxidation. Environmental Science & Technology, 57(11): 4522–4532

Huang S, Jaffé P R (2015). Characterization of incubation experiments and development of an enrichment culture capable of ammonium oxidation under iron-reducing conditions. Biogeosciences, 12(3): 769–779

Kao C, Zhang Q, Li J W, Gao R T, Li W Y, Li X Y, Wang S Y, Peng Y Z (2022). Simultaneous nitrogen and phosphorus removal from municipal wastewater by Fe(III)/Fe(II) cycling mediated partial-denitrification/anammox. Bioresource Technology, 363: 127997

Kappler A, Bryce C, Mansor M, Lueder U, Byrne J M, Swanner E D (2021). An evolving view on biogeochemical cycling of iron. Nature Reviews Microbiology, 19(6): 360–374

Kubeneck L J, Rothwell K A, Notini L, Thomasarrigo L K, Schulz K, Fantappiè G, Joshi P, Huthwelker T, Kretzschmar R (2025). *In situ* vivianite formation in intertidal sediments: ferrihydrite-adsorbed P triggers vivianite formation. Environmental Science & Technology, 59(1): 523–532

Le C P, Nguyen H T, Nguyen T D, Nguyen Q H M, Pham H T, Dinh H T (2021). Ammonium and organic carbon co-removal under Feammox-coupled-with-heterotrophy condition as an efficient approach for nitrogen treatment. Scientific Reports, 11(1): 784

Li X, Huang Y, Liu H W, Wu C, Bi W, Yuan Y, Liu X (2018). Simultaneous Fe(III) reduction and ammonia oxidation process in Anammox sludge. Journal of Environmental Sciences, 64: 42–50

Lin J W, Xiang W J, Zhan Y H (2023). Comparison of magnetite, hematite and goethite amendment and capping in control of phosphorus release from sediment. Environmental Science and Pollution Research, 30(24): 66080–66101

Liu Y, Dong J C, Cheng X H, Cen X T, Dang Y, Xu K N, Zheng M (2025). Dual role of organic matter in Feammox-driven nitrogen and phosphate removal. Water Research X, 27: 100312

Lovley D R, Phillips E J P (1986). Organic matter mineralization with reduction of ferric iron in anaerobic sediments. Applied and Environmental Microbiology, 51(4): 683–689

Nguyen H T, Nguyen L D, Le C P, Hoang N D, Dinh H T (2023). Nitrogen and carbon removal from anaerobic digester effluents with low carbon to nitrogen ratios under Feammox conditions. Bioresource Technology, 371: 128585

Pan M, Jiang T, Wang Z H, Huang X Z, Liu S J, Huang X M (2025). Enhanced nitrogen removal via simultaneous nitrification-denitrification (SND) and Feammox in a magnetic zeolite modified intermittently aerated sequential biological reactor. Frontiers of Environmental Science & Engineering, 19(9): 115

Parfitt R L, Atkinson R J, Smart R S C (1975). The mechanism of phosphate fixation by iron oxides. Soil Science Society of America Journal, 39(5): 837–841

Pratt A R (1997). Vivianite auto-oxidation. Physics and Chemistry of Minerals, 25(1): 24–27

Qin H, Nie W B, Yi D, Yang D X, Chen M L, Liu T, Chen Y (2024). Hematite-facilitated microbial ammoxidation for enhanced nitrogen removal in constructed wetlands. Frontiers of Environmental Science & Engineering, 18(7): 82

Rasmussen H, Nielsen P H (1996). Iron reduction in activated sludge measured with different extraction techniques. Water Research, 30(3): 551–558

Wang S X, Huang Y X, Wang H, Lu Y Y, He W L, Li J, Fan N S, Huang B C, Jin R C (2023). A comparative study of different iron minerals on phosphorus capture from municipal wastewater and subsequent recovery as vivianite through acidogenic fermentation. Chemical Engineering Journal, 466: 143370

Wang X M, Liu F, Tan W F, Li W, Feng X H, Sparks D L (2013). Characteristics of phosphate adsorption-desorption onto ferrihydrite: comparison with well-crystalline Fe (hydr)oxides. Soil Science, 178(1): 1–11

Wang X N, Jiang Z, Qian J S, Fu W Y, Pan B C (2024). Structure evolution of iron (hydr)oxides under nanoconfinement and its implication for water treatment. Environmental Science & Technology, 58(1): 826–835

Wilfert P, Kumar P S, Korving L, Witkamp G J, Van Loosdrecht M C M (2015). The relevance of phosphorus and iron chemistry to the recovery of phosphorus from wastewater: a review. Environmental Science & Technology, 49(16): 9400–9414

Xu H, Zhang L, Li Z, Chen Y, Yang B, Zhou Y (2024). Activation of iron oxides through organic matter-induced dissolved oxygen penetration depth dynamics enhances iron-cycling driven ammonium oxidation in microaerobic granular sludge. Water Research, 266: 122400

Xu S M, Zhu S B, Xiong H X (2022). Phosphate adsorption removals by five synthesized isomeric *α-, β-, γ*-FeOOH. Water, Air, & Soil Pollution, 233(11): 454

Yang W H, Weber K A, Silver W L (2012). Nitrogen loss from soil through anaerobic ammonium oxidation coupled to iron reduction. Nature Geoscience, 5(8): 538–541

Yang X R, Li H, Su J Q, Zhou G W (2021). Anammox bacteria are potentially involved in anaerobic ammonium oxidation coupled to iron(III) reduction in the wastewater treatment system. Frontiers in Microbiology, 12: 717249

Yang Y F, Zhang Y B, Li Y, Zhao H M, Peng H (2018). Nitrogen removal during anaerobic digestion of wasted activated sludge under supplementing Fe(III) compounds. Chemical Engineering Journal, 332: 711–716

Ye W Z, Yan J Q, Yan J, Ji Q X, Huang L, Li M, Zhang H G, Hong S Y, Cai J Y (2025). Unveiling the effect of Fe(III) and sulfate on ammonium oxidation under anaerobic condition: interactions and extracellular electron transfer. Water Research, 287: 124517

Zhu B Y, Yuan R F, Wang S N, Chen H L, Zhou B H, Cui Z X, Zhang C Y (2024). Iron-based materials for nitrogen and phosphorus removal from wastewater: a review. Journal of Water Process Engineering, 59: 104952